Journal of Magnetic Resonance **152,** 14–25 (2001)
doi:10.1006/jmre.2001.2393, available online at http://www.idealibrary.com on IDEAL®

Double-Quantum-Filtered Rotational-Resonance MAS NMR in the Presence of Large Chemical Shielding Anisotropies

Matthias Bechmann, Xavier Helluy, and Angelika Sebald[1]

Bayerisches Geoinstitut, Universität Bayreuth, D-95440 Bayreuth, Germany

Received October 30, 2000; revised May 24, 2001

Double-quantum filtration under rotational resonance MAS NMR conditions where the chemical shielding anisotropies involved exceed the differences in isotropic chemical shielding is considered by means of numerical simulations and ^{13}C MAS NMR experiments. The responses of two different pulse sequences, suitable for double-quantum filtration specifically under rotational resonance conditions, to large chemical shielding anisotropies are compared. In the presence of large chemical shielding anisotropies a very recently introduced pulse sequence (T. Karlsson, M. Edén, H. Luthman, and M. H. Levitt, *J. Magn. Reson*. 145, 95–107, 2000) suffers losses in double-quantum-filtration efficiencies. The double-quantum-filtration efficiency of another pulse sequence (N. C. Nielsen, F. Creuzet, R. G. Griffin, and M. H. Levitt, *J. Chem. Phys*. 96, 5668–5677, 1992) is less afflicted by the presence of large chemical shielding anisotropies. Both sequences deliver double-quantum-filtered lineshapes that sensitively reflect chemical shielding tensor orientations. It is further shown that double-quantum-filtered rotational-resonance lineshapes of spin systems composed of more than two spins offer a suitable experimental approach for determining chemical shielding tensor orientations for cases where conventional rotational-resonance experiments are not applicable due to the presence of additional background resonances.

Key Words: **MAS NMR; rotational resonance; double-quantum filtration; numerical simulations; ^{13}C spin systems; chemical shielding tensors.**

INTRODUCTION

Consider a scenario where magic-angle spinning (MAS) NMR techniques are faced with the task of determining a molecular conformational parameter. Further suppose that neither MAS NMR experiments designed for the determination of internuclear distances nor so-called double-quantum (DQ) heteronuclear local field (HLF) experiments (*1*) can solve the problem posed. As an example, consider a carboxylate group and its orientation in an organic molecule, in the absence of structural motifs that would enable DQ-HLF experiments. Obviously, measurements of internuclear ^{13}C –^{13}C distances are also unable to reveal the orientation of this COO group in the molecule. To solve a task of this kind, MAS NMR must rely on ^{13}C chemical shielding tensor orientations. Whenever reasonably accurate assumptions about the relationships between ^{13}C chemical shielding tensor orientations and molecular geometries for a given class of compounds or molecular fragments can be made, knowledge of the mutual orientations of ^{13}C chemical shielding tensors can be translated to the desired information about molecular conformations, for instance, about the orientation of a COO group in an organic molecule.

The rotational-resonance (R^2) condition (*2–8*) makes information about chemical shielding tensor orientations in small, isolated homonuclear spin systems accessible in an experimentally straightforward manner. With a R^2 condition fulfilled (i.e., when the MAS frequency matches an integer multiple of the isotropic chemical shielding difference between two spins, $\omega_{iso}^{\Delta} \approx n\omega_r$, where n is a small integer), all anisotropic interactions are reintroduced into the R^2 MAS NMR spectra. It has been demonstrated that chemical shielding tensor orientations can be reliably extracted from R^2 lineshapes by iterative fitting approaches, based on numerically exact lineshape simulations (*9–13*). This conventional R^2 MAS NMR approach, however, is limited to cases where the (re)coupled spin system is spatially isolated in the crystal lattice and where no additional resonances interfere with the lineshape-analysis procedures. Combining the R^2 MAS NMR approach with double-quantum filtration (DQF) circumvents these severe restrictions on sample properties and considerably broadens the application range of lineshape-based one-dimensional MAS NMR experiments. Most of the currently known, quite numerous MAS NMR recoupling schemes (*1*) that may be employed for R^2-DQF purposes suffer reductions in DQF efficiency as soon as nonnegligible chemical shielding anisotropies (csa) are involved. The presence of considerable csa, preferably under conditions of relatively slow MAS, however, forms the basis of a problem-solving strategy for the scenario mentioned above.

The purpose of this study is to investigate how well csa orientational parameters may be derived from experimental R^2-DQF lineshapes. We will do so by means of numerical simulations and ^{13}C MAS NMR experiments. Different ^{13}C isotopomers of three different compounds will be used (see Fig. 1). The crystal

[1] To whom correspondence should be addressed. E-mail: angelika.sebald@uni-bayreuth.de.

1090-7807/01 $35.00

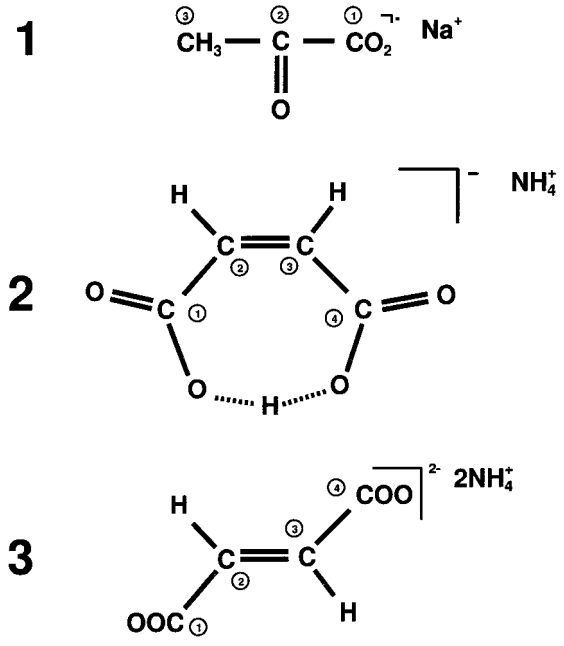

FIG. 1. Schematic representation of the molecular structures of **1**, **2**, and **3**; the numbering scheme of the carbon atoms is used throughout. It is identical to the numbering schemes in the description of the crystal structures of **1** (*14*) and **2** (*15*), but differs from that used in the description of the crystal structure of **3** (*16*).

structures of **1** (*14*), **2** (*15*), and **3** (*16*), as well as all parameters of the ^{13}C spin systems of **1** (*12*) and **2** (*11*) are known. The known parameters of the ^{13}C spin systems of **1** and **2** will serve to study the properties of two different R^2-DQF pulse experiments (*17, 18*) in the presence of considerable csa. Criteria for the selection of these two pulse sequences were the ease and robustness of their experimental implementation, the absence of potentially limiting ^{1}H-decoupling requirements, and the narrowbandedness of the R^2 condition, which holds promise for some naturally occurring degrees of selectivity in multiple spin systems. Finally, we will determine the so far unknown ^{13}C chemical shielding tensor orientations of **3** from ^{13}C R^2-DQF lineshapes of a fully ^{13}C-enriched sample of diammonium fumarate.

EXPERIMENTAL

Samples

The sodium pyruvate samples used in this study are commercially available (**1**, with ^{13}C in natural abundance (Aldrich Chemicals); **1-C1/C2**, selectively ^{13}C1, ^{13}C2-enriched sodium pyruvate (Isotec Inc.)). The educts (maleic anhydride and fumaric acid: natural ^{13}C abundance (Aldrich Chemicals); ^{13}C2, ^{13}C3-enriched, and fully ^{13}C-enriched (Isotec Inc. and CIL)) for the synthesis of various ^{13}C isotopomers of monoammonium maleate (**2**, with ^{13}C in natural abundance) and diammonium fumarate (**3**, with ^{13}C in natural abundance) are also commercially available. **2-C2/C3** (selectively ^{13}C2, ^{13}C3-enriched monoammonium maleate), **2-U^{13}C** (fully ^{13}C-enriched monoammonium maleate), and **3-U^{13}C** (fully ^{13}C-enriched diammonium fumarate) were synthesized by reacting the respective educts with the appropriate amounts of $(NH_4)(HCO_3)$ in aqueous solution under ambient conditions in the dark. In addition, isotopically diluted samples of almost all ^{13}C-enriched compounds were made by cocrystallization of the ^{13}C-enriched compounds with their counterparts with ^{13}C in natural abundance. The ratios of enriched to unenriched materials (by weight) are the following: **1-C1/C2$_{dil}$** 1 : 5, **2-U^{13}C$_{dil}$** 1 : 9, **3-U^{13}C$_{dil}$** 1 : 10. R^2-DQF MAS NMR experiments were run on the diluted and undiluted ^{13}C-enriched samples. In all cases identical R^2-DQF lineshapes for the diluted and undiluted ^{13}C-enriched samples were found. Consequently, the experimental lineshapes obtained from the undiluted ^{13}C-enriched samples were used as experimental data input in lineshape simulations.

^{13}C MAS NMR

^{13}C MAS NMR spectra were recorded on Bruker MSL 100, MSL 200, MSL 300, and DSX 500 NMR spectrometers. The corresponding ^{13}C Larmor frequencies $\omega_0/2\pi$ are -25.2, -50.3, -75.5, and -125.8 MHz. The ^{13}C resonance of $SiMe_4$ serves as the 0 ppm reference of ^{13}C chemical shielding. MAS frequencies were generally in the range $\omega_r/2\pi = 0.8$–10.0 kHz and were actively controlled to within ± 2 Hz. Lineshapes of experimental ^{13}C MAS NMR spectra were checked to be identical when using either Hartmann-Hahn cross-polarization (CP) or ^{13}C single-pulse excitation. ^{13}C R^2-DQF MAS NMR spectra of **3-U^{13}C** for purposes of iterative lineshape fitting were recorded on the DSX 500 NMR spectrometer with ^{13}C $\pi/2$ pulse durations of 4.0 μs and TPPM (*19*) ^{1}H decoupling (amplitude of 83 kHz) applied throughout. ^{13}C MAS NMR experiments on the MSL 100 spectrometer employed 7 mm o.d. ZrO_2 rotors, ^{13}C$\pi/2$ pulse durations of 4.0 μs, and c.w. ^{1}H decoupling amplitudes of 62.5 kHz; on the MSL 200 and MSL 300 spectrometers, 4 mm o.d. ZrO_2 rotors, ^{13}C $\pi/2$ pulse durations of 3.5 μs, and c.w. ^{1}H decoupling amplitudes of 71.4 kHz were used.

Two different pulse sequences for purposes of DQ filtration under R^2 conditions in the presence of considerable chemical shielding anisotropies will be considered. The two pulse sequences chosen are depicted in Fig. 2. Both sequences are experimentally straightforward and robust. The two sequences differ with respect to their highest possible DQF efficiencies in powder samples under ideal conditions, that is, in the presence of dipolar coupling and the absence of csa and isotropic J coupling. The sequence depicted in Fig. 2a (*17*) only depends on the powder angle β_{PR}^D and thus its highest theoretically possible DQF efficiency amounts to 73%. The sequence depicted in Fig. 2b (*18*) has an upper theoretical limit of its DQF efficiency of 50% due its orientation dependence on two angles, β_{PR}^D and γ_{PR}^D. For the sake of brevity, we will refer to the two pulse sequences as

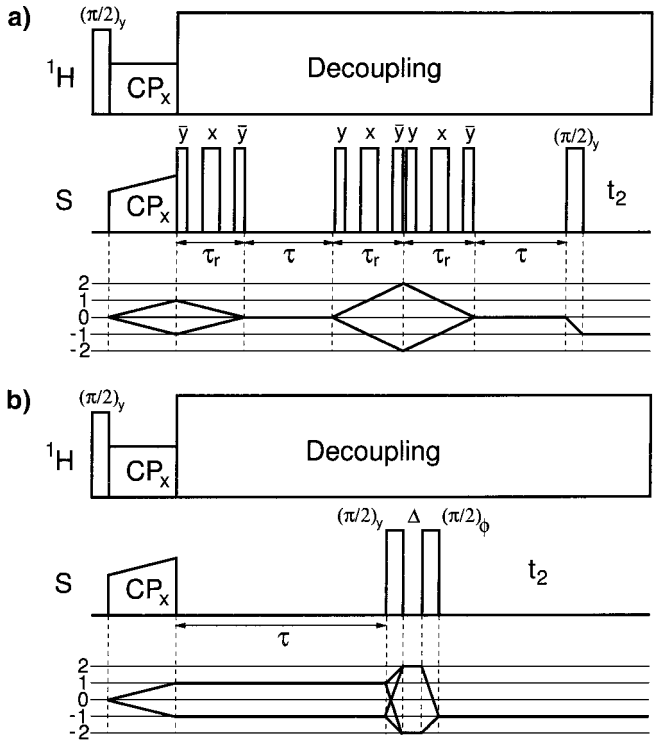

FIG. 2. The pulse sequences and coherence transfer paths of two different R^2-DQF MAS NMR experiments, with cross-polarization. (a) The R^2-DQF$_\beta$ MAS NMR experiment (*17*), where τ_r denotes rotation period, the two periods τ have equal durations, and the three-pulse subsequences consist of equally spaced $\pi/4$–$\pi/2$–$\pi/4$ pulses, spanning one rotation period. (b) The R^2-DQF$_{\beta,\gamma}$ MAS NMR experiment (*18*), consisting of an excitation period τ and two closely spaced $\pi/2$ pulses, separated by a short delay period Δ. Phase cycling follows the standard recipes for DQF (*32*).

R^2-DQF$_\beta$ ((*17*); see Fig. 2a) and R^2-DQF$_{\beta,\gamma}$ ((*18*); see Fig. 2b). Note that the spin-system circumstances considered here are far away from these ideal conditions.

Definitions, Notation, and Numerical Methods

Shielding notation (*20*) is used throughout. For the interactions $\lambda = CS$ (chemical shielding), $\lambda = D$ (direct dipolar coupling), and $\lambda = J$ (indirect dipolar (J) coupling) the isotropic part ω^λ_{iso}, the anisotropy δ^λ, and the asymmetry parameter η^λ relate to the principal elements of the interaction tensor ω^λ as follows (*21*): $\omega^\lambda_{iso} = (\omega^\lambda_{xx} + \omega^\lambda_{yy} + \omega^\lambda_{zz})/3$, $\delta^\lambda = \omega^\lambda_{zz} - \omega^\lambda_{iso}$, and $\eta^\lambda = (\omega^\lambda_{yy} - \omega^\lambda_{xx})/\delta^\lambda$ with $|\omega^\lambda_{zz} - \omega^\lambda_{iso}| \geq |\omega^\lambda_{xx} - \omega^\lambda_{iso}| \geq |\omega^\lambda_{yy} - \omega^\lambda_{iso}|$. For indirect dipolar coupling $\omega^J_{iso} = \pi J_{iso}$, and for direct dipolar coupling $\eta^D = \omega^D_{iso} = 0$ and $\delta^{D_{ij}} = b_{ij} = -\mu_0\gamma_i\gamma_j\hbar/(4\pi r^3_{ij})$, where γ_i, γ_j denote gyromagnetic ratios and r_{ij} is the internuclear distance between spins S_i, S_j. The Euler angles $\Omega_{IJ} = \{\alpha_{IJ}, \beta_{IJ}, \gamma_{IJ}\}$ (*22*) relate axis system I to axis system J, where I, J denote P (principal axis system, PAS), C (crystal axis system, CAS), R (rotor axis system, RAS), or L (laboratory axis system). For lineshape simulations of R^2 MAS NMR spectra of isolated two-spin systems (S_i, S_j) it is convenient to take the PAS of the corresponding dipolar coupling tensor $\omega^{D_{ij}}$ as the CAS, $\Omega^{D_{ij}}_{PC} = \{0, 0, 0\}$.

Suitable numerical simulation approaches must be exact as well as efficient. Especially when unknown parameters are to be determined by means of iterative (lineshape) fitting methods, numerical efficiency becomes crucial. For the in-depth numerical analysis of conventional R^2 MAS NMR spectra, the REPULSION (*23*) or Lebedev (*24*) schemes for the calculation of powder averages, together with some routines of the GAMMA package (*26*) and the use of COMPUTE (*26*) or γ-COMPUTE approaches (*27–29*), yield sufficient computational efficiency to enable these calculations within reasonable amounts of time on common contemporary PCs (*30*). The situation changes with the need to calculate R^2-DQF spectra. Calculation of the time evolution of the spin dynamics under the pulse sequence now requires the application of the so-called direct method. While direct-method calculations are generally applicable, they are numerically highly inefficient. For example, if the calculation of the conventional R^2 MAS NMR spectrum of a two-spin system, employing the γ-COMPUTE approach, takes 3 s on a given PC, the same calculation takes 20 min when using the direct method. For realistic applications and determinations of unknown parameters from experimental spectra, the latter is too slow. Improvements in the efficiency of the numerical simulations are needed. Two additional features have been included in our simulation programs. We only use the direct method for the calculation of the time evolution where absolutely necessary, and switch to COMPUTE (*26*) where possible. For the calculation of R^2-DQF spectra, the calculation may be divided into a direct-method part during the execution of the pulse sequence, and a COMPUTE part during the acquisition of the FID. This "mixed method" offers considerable savings as long as the FID occupies the larger part of the total duration of time over which the calculation must be carried out. Another major potential for accelerating the numerical procedures lies in the possibilities of parallel computing. Regarding numerical simulations of MAS NMR spectra of polycrystalline powder samples, the most obvious and straightforward part in the calculations that lends itself to the advantages of parallel-computing code is the calculation of the powder averages (*31*). Our present implementation makes use of a master/slave program where the master distributes to the slaves a subset of REPULSION angles as soon as slaves become idle and where each slave computes the NMR subspectrum corresponding to the subset of REPULSION angles it received from the master. At the end, the master sums up all the subspectra computed by the slaves. This parallel-computing code for powder averaging was implemented using the Parallel Virtual Machine (PVM) library (*33*) and currently runs on a Linux cluster with eight dual 450 MHz Intel Pentium processor PCs. A general impression of the various contributions to the reduction of computational times may be obtained from Table 1. The computional times quoted in Table 1 refer to the abovemoted Linux cluster. They are valid for the calculation of R^2-DQF$_{\beta,\gamma}$ spectra of 2-, 3-, and 4-spin systems, where a set of 376 REPULSION

TABLE 1
Typical Times [s] Required to Calculate R^2-DQF Spectra (See Text for Details) of 2-, 3-, and 4-Spin Systems[a]

	2-spin system	3-spin system	4-spin system
Direct method, single processor	8016	[b]	[b]
Mixed method, single processor	291	1454	9395
Mixed method, parallel mode	23	100	654

[a] See text for a description of the Linux cluster used. The savings in parallel mode are only slightly less than the values expected when dividing the single-processor-based durations by the number (16 in our case) of CPUs used.
[b] Not determined.

(*23*) powder angles, a duration of $\tau = 1$ ms, and a FID lasting for 17 ms have been assumed. Some simulations reported in this study were carried out in single-processor mode, while calculations of error scans and planes, R^2-DQF efficiency curves, and iterative lineshape fits employed parallel computing. For iterative minimizations, our simulation programs are combined with the optimization routines of the MINUIT package (*34*).

RESULTS AND DISCUSSION

The following is organized in three sections. The first section examines the performance of the R^2-DQF$_\beta$ experiment ((*17*), Fig. 2a) in the presence of large chemical shielding anisotropies; this part takes advantage of the known parameters of the ^{13}C spin system in sodium pyruvate, **1** (*12*). The second section deals in a similar manner with the properties of the R^2-DQF$_{\beta,\gamma}$ experiment ((*18*), Fig. 2b), including the $n = 0$ R^2 condition encountered in various, fully characterized, ^{13}C isotopomers of monoammonium maleate, **2** (*11*). The third section is devoted to the determination of the ^{13}C chemical shielding tensor orientations in the fumarate anion in diammonium fumarate, **3**, from ^{13}C R^2-DQF$_{\beta,\gamma}$ lineshapes of **3-U^{13}C**.

The R^2-DQF$_\beta$ MAS NMR Experiment in the Presence of csa

For the R^2-DQF$_\beta$ MAS NMR experiment (*17*) it has been demonstrated that experimental lineshapes can be reproduced well numerically and reflect the anisotropic interaction parameters of a given spin system with similar sensitivities as the corresponding conventional R^2 lineshapes (*12*). This demonstration employed the ^{13}C2–^{13}C3 spin pair in selectively ^{13}C-labeled sodium pyruvate, **1-C2/C3**, under the $n = 1$ R^2 condition. This spin pair is characterized by a large difference in isotropic chemical shielding values ($\omega_{iso}^{\Delta_{23}} = 176.8$ ppm), and a small chemical shielding anisotropy of ^{13}C3 ($\delta^{CS_3} = 0.14\ \omega_{iso}^{\Delta_{23}}$). Under these conditions b_{23} is by far the most sensitively encoded parameter in the $n = 1$ R^2 as well as in the R^2-DQF$_\beta$ lineshapes. In addition, for the parameters describing the spin pair in **1-C2/C3** a maximum $n = 1$ R^2-DQF$_\beta$ efficiency of 47% was predicted numerically, while 35% were found experimentally (both at a Larmor frequency $\omega_0/2\pi = -50.3$ MHz).

We continue to use the ^{13}C spin system in solid sodium pyruvate, but now switch to **1-C1/C2**. The most prominent features of this spin pair are a large dipolar coupling constant b_{12} ($b_{12}/2\pi = -2004$ Hz), a small difference in isotropic chemical shielding ($\omega_{iso}^{\Delta_{12}} = 37.3$ ppm), and large csa at both ^{13}C sites ($\delta^{CS_1} = 2.20\omega_{iso}^{\Delta_{12}}$, $\delta^{CS_2} = 2.95\omega_{iso}^{\Delta_{12}}$). Figure 3 displays a selection of different experimental R^2-DQF$_\beta$ spectra of **1-C1/C2** in comparison with the corresponding simulated spectra, employing the known spin-pair parameters of **1-C1/C2** (*12*). The spectra shown in Fig. 3 emphasize two points: (i) The R^2-DQF$_\beta$ lineshapes are very sensitive to the choice of the experimental parameter τ (while slight misjudgments of the pulse durations by up to ca. 0.3 μs are found to have no significant impact on the resulting lineshapes). (ii) The simulated spectra, based on the known parameters of the spin pair in **1-C1/C2**, reproduce well the experimentally observed R^2-DQF$_\beta$ lineshapes. With our original goal in mind, that is, the determination of molecular conformations based on csa tensor orientations, we need to examine in more detail how sensitively the Euler angles $\Omega_{PC}^{CS_{i,j}}$, $i, j = 1, 2$ are encoded in these lineshapes.

This examination follows a purely numerical approach and is illustrated in Fig. 4. First, a R^2 spectrum based on the experimentally determined best-fit parameters of the spin pair in **1-C1/C2** (*12*) is calculated, followed by one-dimensional error scans for each of the Euler angles $\Omega_{PC}^{CS_{i,j}}$. The resulting error curves for this

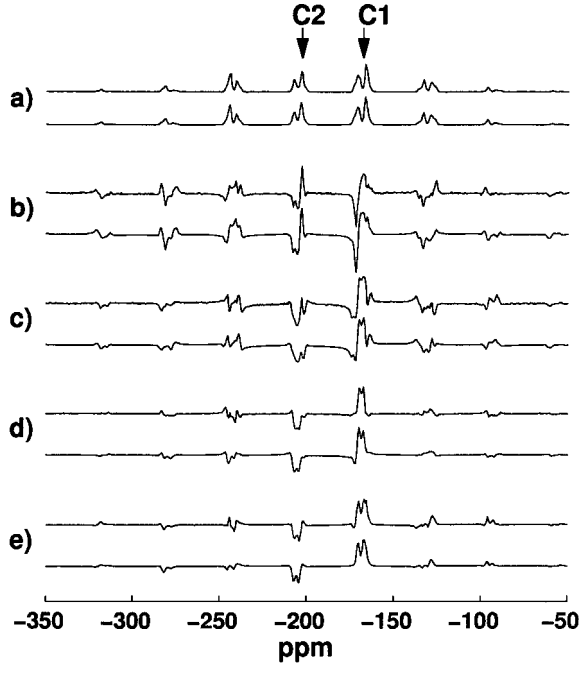

FIG. 3. Comparison of experimental (top traces) and simulated (bottom traces) ^{13}C $n=1$ R^2 and R^2-DQF$_\beta$ lineshapes of the spin pair in **1-C1/C2** at $\omega_0/2\pi = -75.5$ MHz and $\omega_r/2\pi = 2793$ Hz; the simulations employ the known parameters of this spin pair (*12*). (a) Conventional R^2 spectra of **1-C1/C2**; arrows indicate the isotropic chemical shielding of ^{13}C1, ^{13}C2. (b–e) R^2-DQF$_\beta$ spectra of **1-C1/C2**, where $\tau = 0.1$ ms (b), $\tau = 0.3$ ms (c), $\tau = 0.5$ ms (d), and $\tau = 0.7$ ms (e).

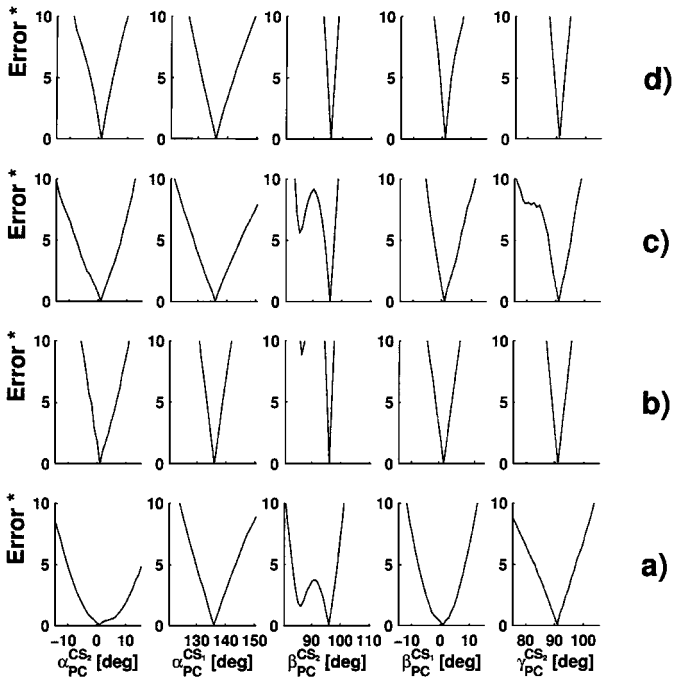

FIG. 4. One-dimensional error scans, illustrating the sensitivity of conventional $n = 1$ R^2 and R^2-DQF$_\beta$ lineshapes to the Euler angles $\Omega_{PC}^{CS_{1,2}}$ in **1-C1/C2** at $\omega_0/2\pi = -75.5$ MHz and $\omega_r/2\pi = 2793$ Hz. The error scans are based on simulated spectra according to the parameters of the spin pair in **1-C1/C2**, so that each individual error scan addresses the situation where all other parameters are at precisely their optimum values. (a) Error scans for the conventional R^2 lineshape. (b–d) Error scans for the R^2-DQF$_\beta$ lineshapes with $\tau = 0.1$ ms (b), $\tau = 0.7$ ms (c), and $\tau = 2.0$ ms (d). The vertical axes in the plots are defined as

$$\text{Error}^* = \sqrt{\frac{\sum_i [(s(i) - ref(i)]^2}{\sum_i [ref(i)]^2}} \cdot 100.$$

This purely numerical comparison can give only an impression of ideal circumstances, in the absence of any (unavoidable) experimental imperfections.

purely numerical conventional R^2 spectrum are shown in Fig. 4a as a reference. The same procedure is then carried out with several numerically simulated R^2-DQF$_\beta$ spectra for a range of different values of τ. The one-dimensional error curves for the five Euler angles $\Omega_{PC}^{CS_{i,j}}$ resulting from these numerically generated R^2-DQF$_\beta$ spectra are depicted in Figs. 4b–d. Obviously, these virtual experiments indicate that for a whole range of values τ the Euler angles $\Omega_{PC}^{CS_{i,j}}$ might be slightly more sensitively encoded in the R^2-DQF$_\beta$ lineshapes than in the conventional R^2 lineshapes. In practice, based on lineshape fitting of real experimental R^2-DQF$_\beta$ spectra, we have been unable to refine the csa orientational parameters of the spin pair in **1-C1/C2** beyond the precision previously obtained from conventional R^2 lineshapes (*12*).

As far as the sensitivities of the lineshape-fit parameters $\Omega_{PC}^{CS_{i,j}}$ are concerned, the R^2-DQF$_\beta$ experiment in the presence of considerable csa's is promising, but less so when considering the achievable R^2-DQF$_\beta$ efficiencies under these conditions. In Fig. 5a the R^2-DQF$_\beta$ efficiencies for **1-C1/C2** are plotted as a function of τ, the expected simulated efficiency curve (—) is compared to the experimentally measured curve (○). The theoretically highest possible efficiency of 9% for this spin pair is predicted to occur at $\tau = 0.7$ ms , while 6% are reached experimentally. The strong fluctuations in R^2-DQF$_\beta$ efficiency as a function of τ lead to relative maxima not only at or near values of τ that are multiples of the rotation period. This feature makes it rather difficult to select optimum experimental parameters in a realistic application situation, unless all parameters of the spin system are known in advance and the best choice of τ can thus be predicted from numerical simulations. A sharp drop in DQF efficiency accompanying the presence of nonnegligible csa from the theoretically highest possible efficiencies under "ideal circumstances" is nothing unique to the R^2-DQF$_\beta$ experiment. This problem afflicts, more or less, many pulse sequences suitable for DQF experiments on polycrystalline powders under MAS conditions. When the R^2-DQF$_\beta$ experiment was originally introduced (*17*), it was pointed out that the presence of csa will generally degrade the DQF efficiency of the experiment. It was further moted that replacing the first three-pulse subsequence (the inversion subsequence, see Fig. 2a) by more sophisticated inversion sequences might improve efficiency matters in the presence of csa. This idea can be tested by numerical simulations. Numerically it is easy to produce not just an improved, but a perfect, inversion condition at the beginning of the pulse sequence. As can be seen in Fig. 5b, again for the parameters of the **1-C1/C2** spin pair, an assumed perfect inversion situation smoothes the oscillations in the R^2-DQF$_\beta$ efficiency as a function of τ, but only slightly boosts the overall R^2-DQF$_\beta$ efficiency in the presence of large csa's.

For very trivial but important reasons of experimentally achievable signal-to-noise ratio, it is desirable to have additional experimental options where informative R^2-DQF lineshapes are obtained with higher efficiencies in the presence of large csa's (i.e., when $\delta^{CS_{i,j}} \geq 2\omega_{iso}^{\Delta_{ij}}$), and where it is easier to predict suitable experimental conditions without extensive advance knowledge of all spin-system parameters.

The R^2-DQF$_{\beta,\gamma}$ MAS NMR Experiment in the Presence of csa

At a first glance, it may seem surprising that we explore the practical performance of the R^2-DQF$_{\beta,\gamma}$ MAS NMR experiment (Fig. 2b), a pulse sequence that is characterized by a considerably lower limit (50%) of its highest theoretical R^2-DQF efficiency under ideal circumstances (*18*). However, the presence of large chemical shielding anisotropies presents rather "nonideal circumstances," leading to less obvious choices of the most suitable experimental approach.

Again, we take the ^{13}C spin pair in **1-C1/C2** as the model case. Figure 5c compares the numerically expected to the experimentally observed R^2-DQF$_{\beta,\gamma}$ efficiencies for this spin pair, plotted as a function of τ. This comparison yields two arguments for the R^2-DQF$_{\beta,\gamma}$ experiment for spin systems with large csa's. First, the optimum choice of experimental values τ is easily predictable, as maxima of the DQF efficiency occur only for values of τ very close to integer multiples of the rotation

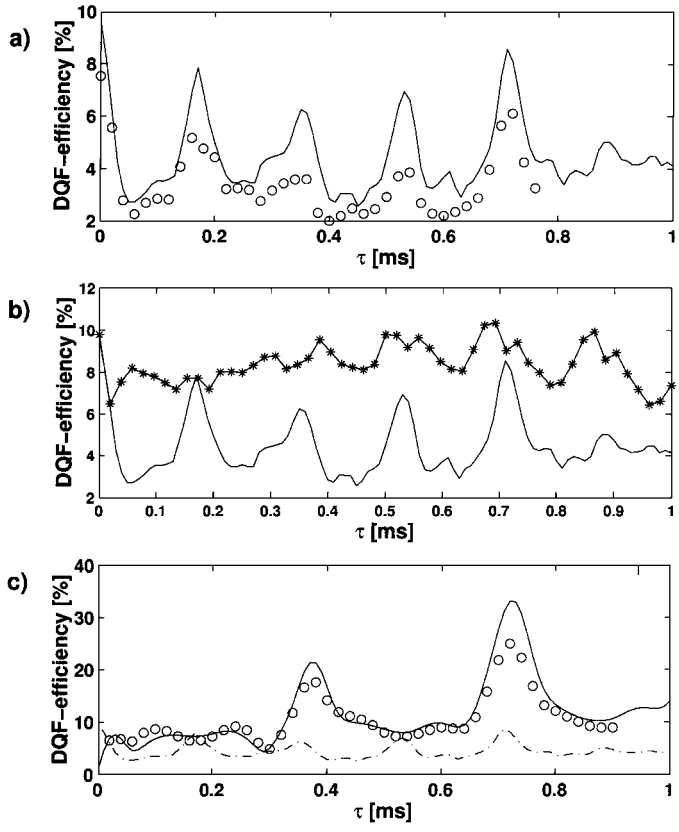

FIG. 5. Numerically predicted and experimentally observed ^{13}C R^2-DQF efficiencies for the ^{13}C spin pair in **1-C1/C2** at $\omega_0/2\pi = -75.5$ MHz and $\omega_r/2\pi = 2793$ Hz. (a) Plot of numerically predicted (—) and experimentally observed (○) $n = 1$ R^2-DQF$_\beta$ efficiencies as a function of τ. (b) Plot of numerically predicted R^2-DQF$_\beta$ efficiencies as a function of τ, where (—) refers to assuming the three-pulse inversion subsequence (see Fig. 2a) inverting the less shielded ^{13}C2 resonance, and (*) refers to assuming perfect inversion at the beginning of the pulse sequence. (c) Plot of numerically predicted (—) and experimentally observed (○) $n = 1$ R^2-DQF$_{\beta,\gamma}$ efficiencies as a function of τ. Also shown are the corresponding numerically predicted (–·–·) $n = 1$ R^2-DQF$_\beta$ efficiencies.

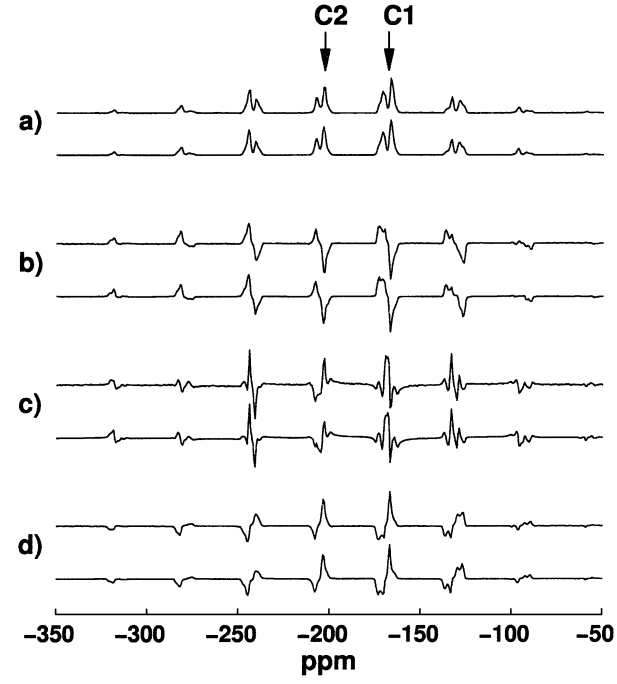

FIG. 6. Comparison of experimental (top traces) and simulated (bottom traces) ^{13}C $n = 1$ R^2 and R^2-DQF$_{\beta,\gamma}$ lineshapes of the spin pair in **1-C1/C2** at $\omega_0/2\pi = -75.5$ MHz and $\omega_r/2\pi = 2793$ Hz; the simulations employ the known parameters of this spin pair (*12*). (a) Conventional R^2 spectra of **1-C1/C2**; arrows indicate the isotropic chemical shielding of ^{13}C1, ^{13}C2. (b–d) R^2-DQF$_{\beta,\gamma}$ spectra of **1-C1/C2**, where $\tau = 0.36$ ms (b), $\tau = 0.54$ ms (c), and $\tau = 0.72$ ms (d).

period. Second, the efficiency maxima are considerably higher than for the R^2-DQF$_\beta$ MAS NMR experiment under otherwise identical conditions. The highest R^2-DQF$_{\beta,\gamma}$ efficiencies for the ^{13}C spin pair in **1-C1/C2** (33% theoretical, 26% experimental at $\tau = 0.72$ ms and $\omega_0/2\pi = -75.5$ MHz; see Fig. 5c) are quite reasonable. Experimental ^{13}C R^2-DQF$_{\beta,\gamma}$ lineshapes of **1-C1/C2** are well reproduced numerically by the known parameters of this spin pair, as can be seen in Fig. 6. Closer inspection of the sensitivity of the R^2-DQF$_{\beta,\gamma}$ lineshapes to the ^{13}C1, ^{13}C2 chemical shielding tensor orientations in **1-C1/C2** reveals that the Euler angles $\Omega_{PC}^{CS_{1,2}}$ are about equally sensitively encoded as in the corresponding conventional R^2 lineshapes. This comparison is depicted in Fig. 7, where the purely numerical exploration from Fig. 4, employing the parameters of the ^{13}C spin pair in **1-C1/C2** for the calculation of one-dimensional error scans is now extended to include the R^2-DQF$_{\beta,\gamma}$ lineshapes and their sensitivities to chemical shielding tensor orientations.

Another useful feature of the R^2-DQF$_{\beta,\gamma}$ experiment is that it also works under the $n = 0$ R^2 condition, as was already

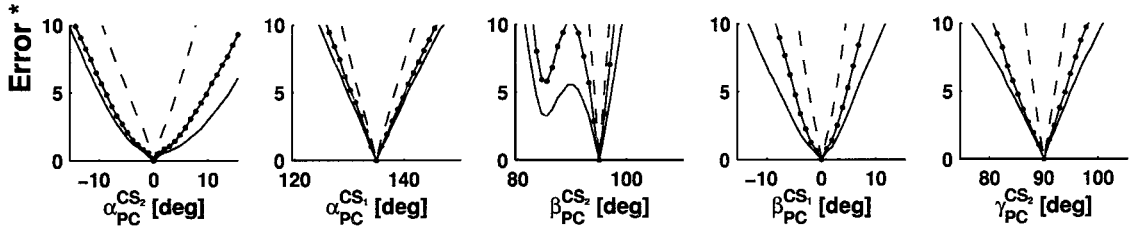

FIG. 7. One-dimensional error scans, illustrating the sensitivity of conventional $n = 1$ R^2 (—), R^2-DQF$_{\beta,\gamma}$ (–·–·), and R^2-DQF$_\beta$ (– – –) lineshapes to the Euler angles $\Omega_{PC}^{CS_{1,2}}$ in **1-C1/C2** at $\omega_0/2\pi = -75.5$ MHz and $\omega_r/2\pi = 2793$ Hz. The procedure is the same as described in the legend of Fig. 4. The error curves are calculated for values of $\tau = 0.30$ ms for the R^2-DQF$_\beta$ sequence and $\tau = 0.72$ ms for the R^2-DQF$_{\beta,\gamma}$ sequence.

demonstrated for the ^{13}C spin pair in diammonium oxalate monohydrate in the original paper describing the experiment (*18*), with roughly 15% R^2-DQF$_{\beta,\gamma}$ efficiency reported for this spin pair at a relatively low MAS frequency ($\omega_0/2\pi = -79.9$ MHz, $\omega_r/2\pi = 1560$ Hz, $\tau = 2\tau_r = 1.28$ ms). Another $n = 0$ R^2 case is encountered in the ^{13}C spin pair in the maleate anion in **2-C2/C3**: here the two ^{13}C chemical shielding tensors are related by mirror-plane symmetry, in the former spin pair a twofold symmetry axis relates the two sites. The known parameters of the spin pair in **2-C2/C3** (*11*) yield simulations of R^2-DQF$_{\beta,\gamma}$ spectra that match the experimentally observed lineshapes very well (see Fig. 8a). Also under the $n = 0$ R^2 condition

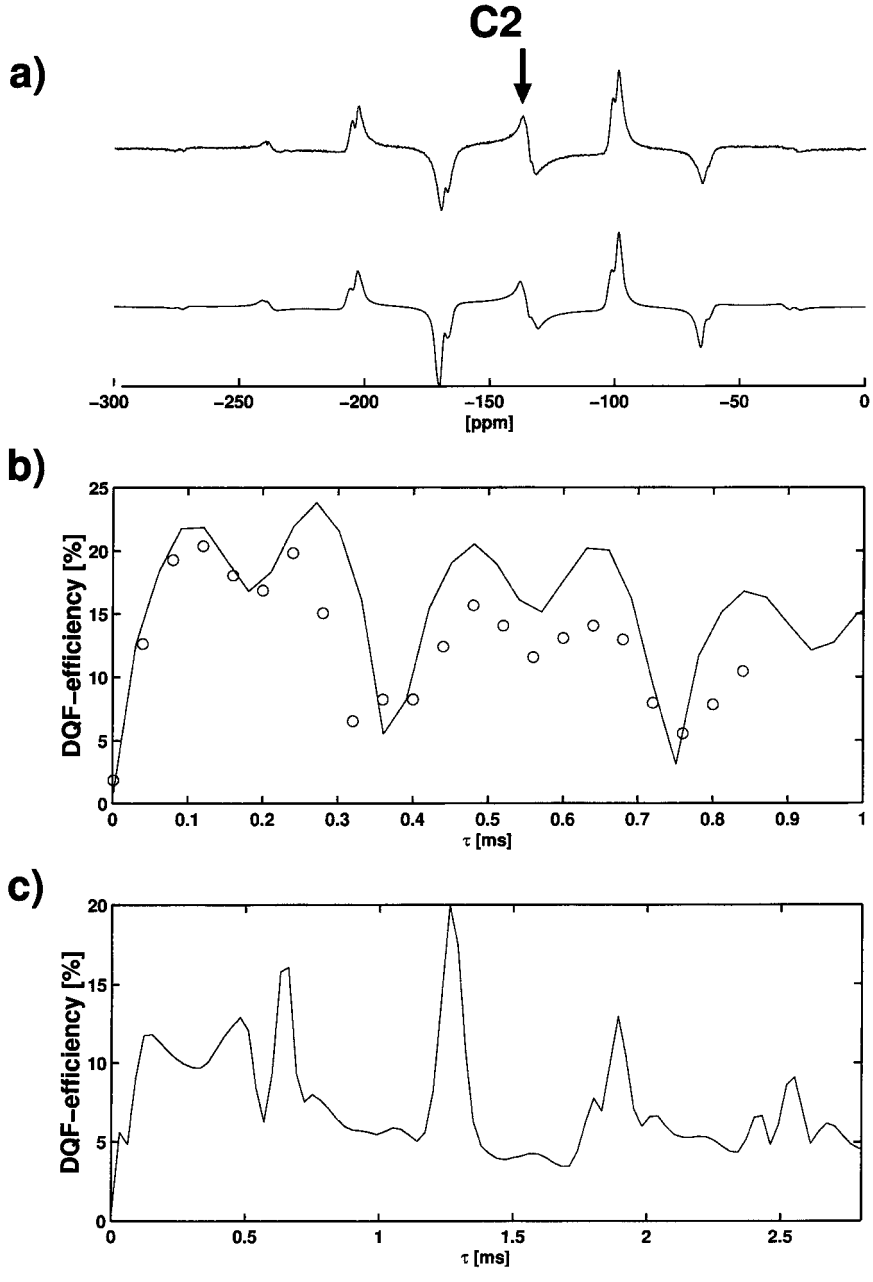

FIG. 8. ^{13}C R^2-DQF$_{\beta,\gamma}$ experiments at the $n = 0$ R^2 condition. (a) Experimental (top) and simulated (bottom) $n = 0$ R^2-DQF$_{\beta,\gamma}$ spectra of **2-C2/C3** at $\omega_0/2\pi = -75.5$ MHz, $\omega_r/2\pi = 2626$ Hz, and $\tau = 0.12$ ms; the simulation employs the known parameters of this spin pair (*11*), the arrow indicates the isotropic ^{13}C2, ^{13}C3 chemical shielding. (b) Numerically predicted (—) and experimentally observed (○) $n = 0$ R^2-DQF$_{\beta,\gamma}$ efficiencies as a function of τ, for **2-C2/C3** at $\omega_0/2\pi = -75.5$ MHz and $\omega_r/2\pi = 2626$ Hz; note the mirror-plane symmetry of **2-C2/C3** and the minima in the R^2-DQF efficiency at $\tau = N\tau_r$. (c) Numerically predicted R^2-DQF$_{\beta,\gamma}$ efficiencies as a function of τ, for the ^{13}C spin pair in diammonium oxalate monohydrate (*18*); note the C_2 symmetry of this spin system and the occurrence of maxima in the R^2-DQF efficiency at $\tau = N\tau_r$.

in the presence of large csa's, fairly high R^2-DQF$_{\beta,\gamma}$ efficiencies can be achieved, but under the $n=0$ R^2 condition the maxima in the efficiency as a function of τ are less obviously related to the rotation period than under the $n=1$ R^2 condition (*35*). This is illustrated in Figs. 8b and c. In Fig. 8b the theoretically expected (—) and the experimentally observed (○) R^2-DQF$_{\beta,\gamma}$ efficiencies for the **2-C2/C3** spin pair are plotted as a function of τ. Under the $n=0$ R^2 condition involving mirror-plane symmetry, the efficiency is minimal at τ values that are integer multiples, N of the rotation period τ_r. In contrast, the $n=0$ R^2 condition involving C_2 symmetry yields maxima of the efficiency when $\tau = N\tau_r$. This is shown in Fig. 8c, where the theoretically expected R^2-DQF$_{\beta,\gamma}$ efficiency as a function of τ is plotted for the ^{13}C spin pair in diammonium oxalate monohydrate (*18*).

In **2-U^{13}C**, the ^{13}C1–^{13}C4 and the ^{13}C2–^{13}C3 pairs always fulfill the $n=0$ R^2 condition due to the molecular mirror-plane symmetry. If the MAS frequency is chosen such that $\omega_r/2\pi$ fulfills in addition the $n=1$ or $n=2$ R^2 condition between ^{13}C1–^{13}C2 and ^{13}C3–^{13}C4, the resulting conventional ^{13}C R^2 lineshapes sensitively reflect all Euler angles $\Omega_{PC}^{CS_{1,2}}$ in this ^{13}C 4-spin system. The ^{13}C chemical shielding tensor orientations in **2-U^{13}C** deviate slightly, but significantly from the typically assumed orientations. For instance, the directions of the most shielded ^{13}C1, ^{13}C2 tensor components are not exactly perpendicular to the molecular plane, and the directions of the intermediate shielded ^{13}C1, ^{13}C2 tensor components deviate slightly from the ^{13}C1=O and ^{13}C2=^{13}C3 bond directions, respectively (*11*). These minor deviations from the "typical ^{13}C shielding tensor orientation" are sensitively reflected in the conventional $n=2$ R^2 spectral lineshapes of **2-U^{13}C**. This is also true for the corresponding R^2-DQF$_{\beta,\gamma}$ lineshapes. Figure 9a depicts an experimental R^2-DQF$_{\beta,\gamma}$ spectrum of **2-U^{13}C**, obtained at $\omega_0/2\pi = -125.8$ MHz under the $n=2$ R^2 condition with $\tau = 0.453$ ms. The corresponding simulated spectrum in Fig. 9b is based on the best-fit values of the Euler angles $\Omega_{PC}^{CS_{1,2}}$ previously obtained from conventional $n=2$ R^2 spectral lineshapes of **2-U^{13}C** (*11*), the simulated spectrum in Fig. 9c assumes Euler angles $\Omega_{PC}^{CS_{1,2}}$ such that the "typical orientation scenario" would be precisely realized (i.e., the directions of the most shielded tensor components are taken as exactly perpendicular to the molecular plane, and the directions of the intermediate tensor components are assumed to be precisely collinear with the C=C and C=O bond directions, respectively). Clearly, the two simulated R^2-DQF$_{\beta,\gamma}$ spectra are significantly different, despite the relative small differences in Euler angles $\Omega_{PC}^{CS_{1,2}}$ between them. The simulated spectrum in Fig. 9b agrees much better with the experimental R^2-DQF$_{\beta,\gamma}$ spectrum than the typical orientation scenario simulation in Fig. 9c. Obviously, exerimental R^2-DQF$_{\beta,\gamma}$ spectra not only of spin pairs but also of spin systems composed of more than two spins may well serve as the starting point for the determination of chemical shielding tensor orientations.

*The ^{13}C Chemical Shielding Tensors in Diammonium Fumarate, **3***

The ^{13}C chemical shielding tensor orientations in diammonium fumarate, **3**, are not known, but various ^{13}C isotopomers of diammonium fumarate have been adopted as model compounds to illustrate the performance of novel MAS NMR pulse sequences and recoupling schemes (*36–39*). The crystal structure of **3** (*16*) explains the difficulties in determining the chemical shielding tensor orientations for **3** by means of conventional ^{13}C R^2MAS NMR experiments. The fumarate anion in solid **3** possesses a center of inversion symmetry, which renders ^{13}C MAS NMR spectra of the pairwise labeled ^{13}C1, ^{13}C4 and ^{13}C2, ^{13}C3 isotopomers uninformative regarding the ^{13}C chemical shielding tensor orientations. Further, the limited mutual spatial isolation of the fumarate anions in the crystal lattice of **3** *a priori* discourages the use of undiluted ^{13}C-labeled isotopomers of **3**. The fully ^{13}C enriched fumarate moiety in **3-U^{13}C** (and/or **3-U^{13}C$_{dil}$**) lifts the symmetry-related problems with the pairwise ^{13}C-labeled isotopomers of **3**. A modest difference in isotropic ^{13}C chemical shielding $\omega_{iso}^{\Delta_{12}} = \omega_{iso}^{\Delta_{34}} = 35.6$ ppm in **3** makes $n=1, 2$ R^2 conditions experimentally accessible, where the lineshapes sensitively reflect the ^{13}C chemical shielding tensor orientations. While conventional ^{13}C R^2 lineshapes of **3-U^{13}C$_{dil}$** are not suitable for purposes of iterative lineshape fitting, the corresponding R^2-DQF lineshapes eliminate the problem of natural-abundance ^{13}C background resonances. Above we have demonstrated that indeed the (known) ^{13}C chemical shielding tensor orientations of the closely related ^{13}C 4-spin system in **2-U^{13}C** are sensitively encoded in the R^2-DQF lineshapes. We are now ready to determine the ^{13}C chemical shielding tensor orientations in the fumarate moiety of diammonium fumarate.

Of the numerous parameters characterizing the ^{13}C 4-spin system in **3-U^{13}C**, many can be determined independently. The known crystal structure of **3** (*16*) yields magnitudes and orientations of the dipolar coupling interaction tensors $\omega^{D_{ij}}$, while solution-state ^{13}C NMR spectra of **3-U^{13}C** provide the values of the isotropic *J*-coupling constants (see Table 2). Isotropic ^{13}C chemical shielding values and the magnitudes of the ^{13}C chemical shielding tensors are obtained from ^{13}C MAS NMR experiments on **3** (see Table 3). The inversion symmetry of the fumarate anion in **3** reduces the number of Euler angles, needed to describe the orientation of the four ^{13}C chemical shielding tensors, to six ($\alpha_{PC}^{CS_i}$, $\beta_{PC}^{CS_i}$, $\gamma_{PC}^{CS_i}$; $i=1,2$). These are the remaining six unknown parameters which must be determined by iterative fitting of ^{13}C R^2-DQF lineshapes. The very first practical step is devoted to the decision whether or not ^{13}C R^2-DQF spectra of the undiluted sample **3-U^{13}C** can serve as experimental input data for the numerical minimization. Experimentally we find identical R^2-DQF lineshapes for **3-U^{13}C** and **3-U^{13}C$_{dil}$** under a variety of experimental conditions. Accordingly, experimental ^{13}C R^2-DQF spectra of **3-U^{13}C** may serve as experimental input

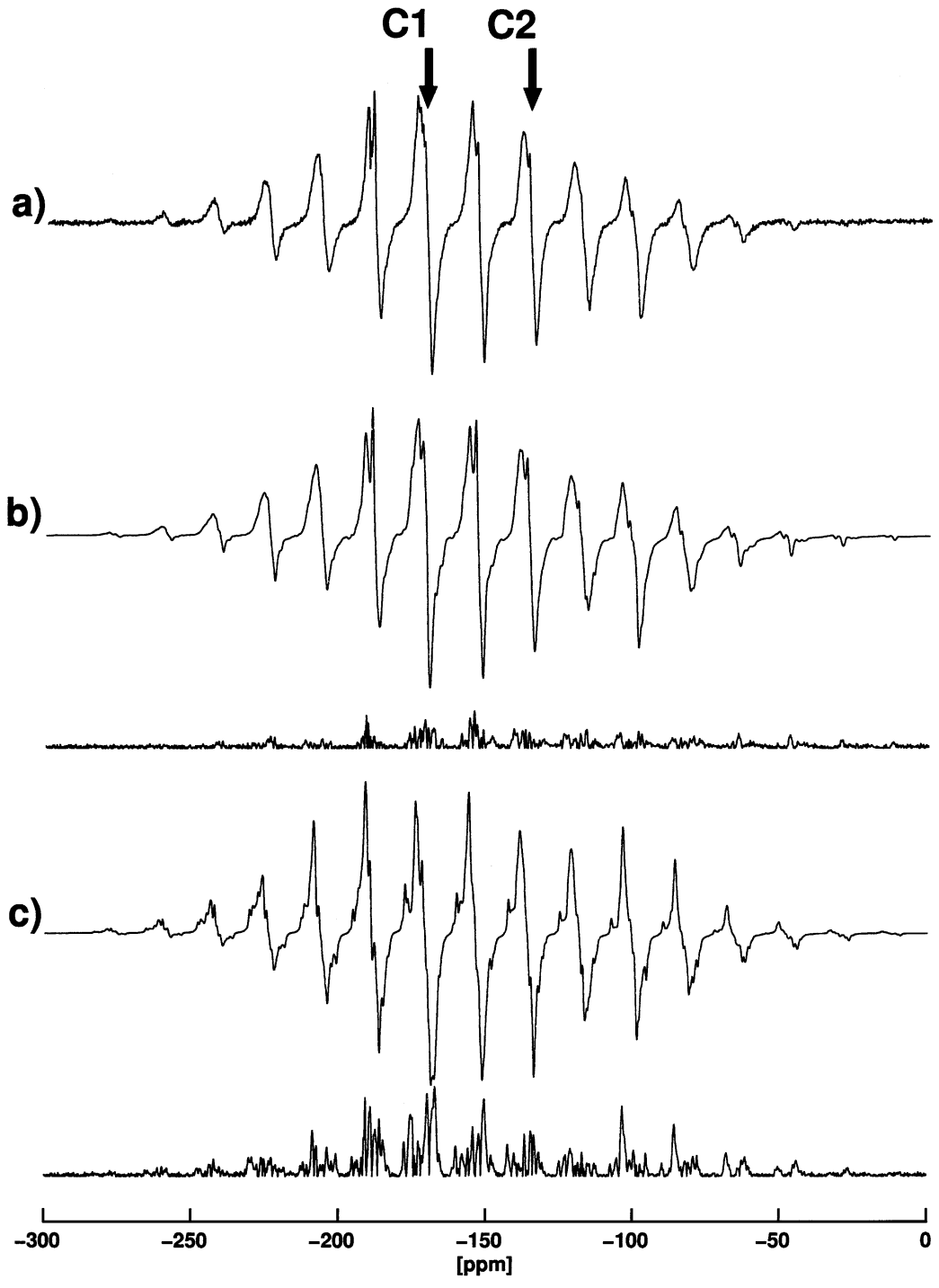

FIG. 9. Comparison of experimental (a) and simulated (b, c) ^{13}C $n = 2$ R^2-DQF$_{\beta,\gamma}$ spectra of **2-U^{13}C** at $\omega_0/2\pi = -125.8$ MHz, $\omega_r/2\pi = 2207$ Hz, and $\tau = 0.453$ ms; the arrows indicate the ^{13}C2, ^{13}C3 and ^{13}C1, ^{13}C4 isotropic chemical shielding regions. The simulated spectrum b is based on the best-fit ^{13}C chemical shielding tensor orientations derived from conventional $n = 2$ R^2 spectra of **2-U^{13}C** (*11*). The simulated spectrum c assumes Euler angles $\Omega_{PC}^{CS_{i,j}}$ corresponding to the "typical csa orientation" scenario (see text). Also shown are the difference curves between experimental and calculated spectra a, b, and a, c, respectively.

data. The results of subsequent iterative lineshape fits are summarized in Table 3 and Fig. 10. The experimental R^2-DQF$_{\beta,\gamma}$ spectrum of **3-U^{13}C**, obtained at $\omega_0/2\pi = -125.8$ MHz under the $n = 2$ R^2 condition with $\tau = 0.446$ ms (Fig. 10a) agrees very well with the simulated spectrum, based on the best-fit values of $\Omega_{PC}^{CS_{1,2}}$ (Fig. 10b). The simulated spectrum, based on a typical csa orientation assumption (Fig. 10c) disagrees significantly with the spectra shown in Figs. 10a and b, even though the best-fit

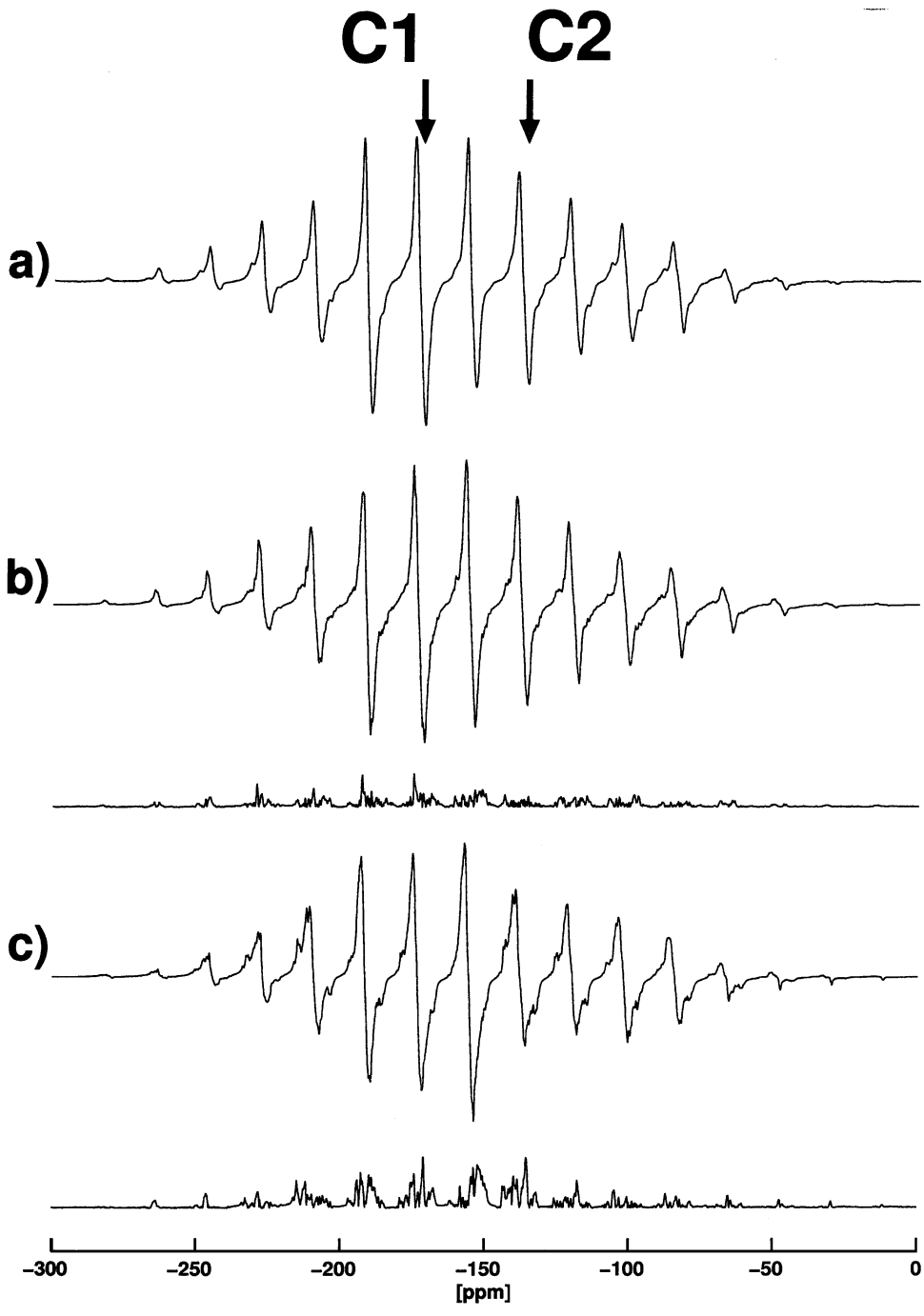

FIG. 10. Comparison of experimental (a) and simulated (b, c) ^{13}C $n = 2$ R^2-DQF$_{\beta,\gamma}$ spectra of **3-U^{13}C** at $\omega_0/2\pi = -125.8$ MHz, $\omega_r/2\pi = 2240$ Hz, and $\tau = 0.446$ ms; the arrows indicate the ^{13}C1, ^{13}C4 and ^{13}C2, ^{13}C3 isotropic chemical shielding regions. The simulated spectrum b is based on the best-fit ^{13}C chemical shielding tensor orientations derived from the experimental spectrum a. The simulated spectrum c assumes Euler angles $\Omega_{PC}^{CS_{i,j}}$ corresponding precisely to a "typical csa orientation" scenario. Also shown are the difference curves between experimental and calculated spectra a, b, and a, c, respectively.

values of $\Omega_{PC}^{CS_{1,2}}$ do not deviate much from the Euler angles corresponding to the typical csa orientations (see Table 3). In addition, the best-fit values of $\Omega_{PC}^{CS_{1,2}}$ equally well reproduce experimental R^2-DQF spectra of **3-U^{13}C** obtained under other experimental conditions. Figures 9 and 10 underscore the importance of a very good signal-to-noise ratio in experimental spectra that serve for purposes of iterative lineshape fitting. Figures 9 and 10 further illustrate the similarities of the four-^{13}C spin systems in **2-U^{13}C** and **3-U^{13}C**: in both cases the R^2-DQF lineshapes reveal small, but significant, deviations of the ^{13}C chemical shielding tensor

TABLE 2
Direct and Indirect Dipolar ^{13}Ci–^{13}Cj Couplings in Diammonium Fumarate, 3

	$ij = 12$ or 34	$ij = 13$ or 24	$ij = 23$	$i, j = 14$
$b_{ij}/2\pi$ [Hz][a]	−2274	−500	−3355	−130
β_{PC}^{D}[°][a,b]	+56.3	+30.1	0	+39.9
$\omega_{ij}^{J_{iso}}$ [Hz][c]	+64.5	+1.5	+68.0	(±)7.0

[a] Calculated from the known crystal structure of **3** (*16*).
[b] Taking $\Omega_{PC}^{D_{23}} = (0, 0, 0)$.
[c] Determined by solution-state ^{13}C NMR of an acqueous solution of **3-U^{13}C** (Larmor frequency $\omega_0/2\pi = -125.8$ MHz, Bruker DRX 500 NMR spectrometer).

orientations from the typical csa orientations scenario. In relation to the geometry of the fumarate anion in **3**, the best-fit values of the Euler angles $\Omega_{PC}^{CS_{1,2}}$ describe the following ^{13}C chemical shielding tensor orientations. The directions of the most shielded components of the ^{13}C1/^{13}C4 and ^{13}C2/^{13}C3 shielding tensors both deviate from being perpendicular to the molecular C1–C2–C3–C4 plane by 15 and 25°, respectively. The direction of the least shielded component of the ^{13}C1/^{13}C4 shielding tensors subtends an angle of 11° with the C1–C2 and C3–C4 bond directions, respectively. The direction of the least shielded component of the ^{13}C2/^{13}C3 shielding tensors is nearly perpendicular to the C2=C3 bond direction (102°) and nearly lies in the molecular plane (within 8°). The direction of the intermediate shielded component of the ^{13}C2/^{13}C3 shielding tensors deviates by 28° from being collinear with the C2=C3 bond direction.

TABLE 3
^{13}C Chemical Shielding in Diammonium Fumarate, 3

	^{13}C1, ^{13}C4	^{13}C2, ^{13}C3
ω_{iso}^{CS} [ppm]	−173.6	−138.0
δ^{CS} [ppm]	64.8	−94.2
η^{CS}	0.82	0.59
$\alpha_{PC_{23}}^{CS}$[°][a]	-126 ± 28[b]	-65 ± 30[b]
$\beta_{PC_{23}}^{CS}$[°][a]	-75 ± 28[c]	-102 ± 13
$\gamma_{PC_{23}}^{CS}$[°][a]	-93 ± 12	$+9 \pm 12$

[a] Euler angles $\Omega_{PC_{23}}^{CS}$ relate to the principal axis system of the ^{13}C2–^{13}C3 dipolar coupling tensor as the CAS, with its y axis defined as perpendicular to the molecular C1–C2–C3–C4 plane. ^{13}C1/^{13}C4 (and ^{13}C2/^{13}C3) in the fumarate anion of **3** are related by inversion symmetry (*16*), implying identical orientations of the ^{13}C1/^{13}C4 (and ^{13}C2/^{13}C3) chemical shielding tensor directions. The "typical csa orientations" in the fumarate anion of **3** would correspond to Euler angles $\Omega_{PC_{23}}^{CS_1} = (-124, -90, -90)$ and $\Omega_{PC_{23}}^{CS_2} = (-90, -90, 0)$. Uncertainties of the best-fit values $\Omega_{PC_{23}}^{CS}$ are quoted for the range spanning $2e_{\min}^2$ in one-dimensional error scans of each of the individual best-fit parameters.
[b] The error curve in the $2e_{\min}^2$ minimum region in one-dimensional error scans of this parameter is broad and featureless.
[c] The error curve in the $2e_{\min}^2$ minimum region in one-dimensional error scans of this parameter displays a sharp ($-75 \pm 8°$) minimum within a broader curve.

SUMMARY

In concluding, we briefly summarize, in our view, the most important findings of our combined numerical and experimental study.

1. The R^2-DQF$_\beta$ and R^2-DQF$_{\beta,\gamma}$ pulse sequences (*17*, *18*) have experimental and numerical robustness and ease in common.

2. Both pulse sequences considerably expand the practical range of spin systems on which R^2 experiments may be successfully carried out in terms of lineshape simulations but where conventional R^2 lineshapes cannot be used. A general area of application where this is important is, for instance, MAS NMR applications on inorganic solids with spin-1/2 isotopes in low natural abundance (*40*).

3. The R^2-DQF$_\beta$ and R^2-DQF$_{\beta,\gamma}$ pulse sequences complement each other. In the presence of large chemical shielding anisotropies and modest differences in isotropic chemical shielding, the R^2-DQF$_{\beta,\gamma}$ sequence (*18*) is the preferable experimental choice for the determination of chemical shielding tensor orientations from R^2-DQF lineshapes. The R^2-DQF$_\beta$ sequence (*17*) works best where large isotropic chemical shielding differences and small chemical shielding anisotropies are involved, especially including cases with relative small dipolar coupling constants (*12, 17*), and thus is the preferable experimental tool when aiming at the determination of internuclear distances in such spin systems.

4. Provided sufficiently fast and exact numerical methods are available, R^2-DQF experiments can be expanded, in a quantitative and reliable manner, to spin systems composed of more than two spins.

5. Finally, it should be moted that both pulse sequences preserve the narrowbandedness and, hence, selectivity, of the correspondin conventional R^2 condition in multiple-spin systems (*41*).

ACKNOWLEDGMENTS

Financial support of our work by the Deutsche Forschungsgemeinschaft and Aventis Pharma, Paris, France, is gratefully acknowledged. We thank Bruker Analytik GmbH, Rheinstetten, for generous access to the DSX 500 NMR spectrometer, and in particular S. Steuernagel for experimental support. We thank H. Maisel, Bayreuth, for the synthesis of all fumaric and maleic acid salts used in this study, and B.Wrackmeyer, Bayreuth, for recording solution-state ^{13}C NMR spectra of **3-U^{13}C**. Last but not least we thank S. Dusold, Bayreuth, for scientific discussions, for his support in the early stages and his continued interest in the later stages of this project.

REFERENCES

1. For general review articles on recoupling methods under MAS NMR conditions see: (i) A. E. Bennett. R. G. Griffin, and S. Vega, Recoupling of homo- and heteronuclear dipolar interactions in rotating solids, *in* "Solid-State NMR IV: Methods and Applications of Solid-State NMR," Vol. 33, "NMR Basic Principles and Progress" (B. Blümich, Ed.), pp. 1–78, Springer

Verlag, Berlin (1994); (ii) S. Dusold and A. Sebald, Dipolar recoupling under magic-angle-spinning conditions, *in* "Annual Reports on NMR Spectroscopy" (G. Webb, Ed.), Vol. 41, pp. 185–264, Academic Press, London (2000), and references given therein.

2. E. R. Andrew, A. Bradbury, R. G. Eades, and V. T. Wynn, Nuclear cross relaxation induced by specimen rotation, *Phys. Lett*. **4,** 99–100 (1963).
3. D. P. Raleigh, M. H. Levitt, and R. G. Griffin, Rotational resonance in solid state NMR, *Chem. Phys. Lett*. **146,** 71–76 (1988).
4. M. H. Levitt, D. P. Raleigh, F. Creuzet, and R. G. Griffin, Theory and simulations of homonuclear spin pairs in rotating solids, *J. Chem. Phys*. **92,** 6347–6364 (1990).
5. A. Kubo and C. A. McDowell, One- and two-dimensional ^{31}P cross-polarization magic-angle-spinning nuclear magnetic resonance studies on two-spin systems with homonuclear dipolar and *J* coupling, *J. Chem. Phys*. **92,** 7156–7170 (1990).
6. A. Schmidt and S. Vega, The Floquet theory of nuclear magnetic resonance spectroscopy of single spins and dipolar coupled spin pairs in rotating solids, *J. Chem. Phys*. **96,** 2655–2680 (1992).
7. T. Nakai and C. A McDowell, An analysis of NMR spinning sidebands of homonuclear two-spin systems using Floquet theory, *Mol. Phys*. **77,** 569–584 (1992).
8. T. Nakai and C. A McDowell, Application of Floquet theory to the nuclear magnetic resonance spectra of homonuclear two-spin systems in rotating solids, *J. Chem. Phys*. **96,** 3452–3466 (1992).
9. S. Dusold, E. Klaus, A. Sebald, M. Bak, and N. C. Nielsen, Magnitudes and relative orientations of chemical shielding, dipolar, and *J* coupling tensors for isolated ^{31}P-^{31}P spin pairs determined by iterative fitting of ^{31}P MAS NMR spectra, *J. Am. Chem. Soc*. **119,** 7121–7129 (1997).
10. S. Dusold, W. Milius, and A. Sebald, Iterative lineshape fitting of MAS NMR spectra: A tool to investigate homonuclear *J* couplings in isolated spin pairs, *J. Magn. Reson*. **135,** 500–513 (1998).
11. S. Dusold, H. Maisel, and A. Sebald, Magnitudes and orientations of interaction tensors determined from rotational resonance MAS NMR lineshapes of a four-^{13}C spin system, *J. Magn. Reson*. **141,** 78–90 (1999).
12. S. Dusold and A. Sebald, Double-quantum filtration under rotational-resonance conditions: Numerical simulations and experimental results, *J. Magn. Reson.* **145,** 340–356 (2000).
13. D. L. Bryce and R.E Wasylishen, *J. Phys. Chem. A* **104,** 7700–7710 (2000).
14. W. Rach, G. Kiel, and G. Gattow, Untersuchungen über Salze der Pyruvinsäure. 2. Kristallstruktur von Kaliumpyruvat, Neubestimmung der Struktur von Natriumpyruvat, *Z. Anorg. Allg. Chem*. **563,** 87–95 (1988).
15. L. Golic and I. Leban, The crystal structure of ammonium hydrogen maleate, *Croat. Chim. Acta* **55,** 41–45 (1982).
16. H. Hosomi, Y. Ito, and S. Ohba, Ammonium and isopropylammonium salts of the fumaric acid dianion, *Acta Cryst. C* **54,** 142–145 (1998).
17. T. Karlsson, M. Edén, H. Luthman, and M. H. Levitt, Efficient double-quantum excitation in rotational resonance NMR, *J. Magn. Reson.* **145,** 95–107 (2000).
18. N. C. Nielsen, F. Creuzet, R. G. Griffin, and M. H. Levitt, Enhanced double-quantum nuclear magnetic resonance in spinning solids at rotational resonance, *J. Chem. Phys*. **96,** 5668–5677 (1992).
19. A. E. Bennett, C. M. Rienstra, M. Auger, K. V. Lakshmi, and R. G. Griffin, Heteronuclear decoupling in rotating solids, *J. Chem. Phys*. **103,** 6951–6958 (1995).
20. M. H. Levitt, The signs of frequencies and phases in NMR, *J. Magn. Reson*. **126,** 164–182 (1997).
21. U. Haeberlen, High resolution NMR in solids. Selective averaging, *in* "Advances in Magnetic Resonance" (J. S. Waugh, Ed.), Suppl. 1, Academic Press, New York (1976).
22. A. R. Edmonds, "Angular Momentum in Quantum Mechanics," Princeton Univ. Press, Princeton, NJ (1974).
23. M. Bak and N. C. Nielsen, REPULSION, a novel approach to efficient powder averaging in solid-state NMR, *J. Magn. Reson*. **125,** 132–139 (1997).
24. M. Edén and M. H. Levitt, Computation of orientational averages in solid state NMR by Gaussian spherical quadrature, *J. Magn. Reson*. **132,** 220–239 (1998).
25. S. A. Smith, T. O. Levante, B. H. Meier, and R. R. Ernst, Computer simulations in magnetic resonance. An object oriented programming approach, *J. Magn. Reson*. *A* **106,** 75–105 (1994).
26. M. Edén, Y. K. Lee, and M. H Levitt, Efficient simulation of periodic problems in NMR: Application to decoupling and rotational resonance, *J. Magn. Reson*. *A* **120,** 56–71 (1996).
27. T. Charpentier, C. Fermon, and J. Virlet, Efficient time propagation technique for MAS NMR simulation: Application to quadrupolar nuclei, *J. Magn. Reson*. **132,** 181–190 (1998).
28. M. Hohwy, H. Bildsoe, H. J. Jakobsen, and N. C. Nielsen, Efficient spectral simulations in NMR of rotating solids. The γ-COMPUTE algorithm, *J. Magn. Reson*. **136,** 6–14 (1999).
29. M. H. Levitt and M. Edén, Numerical simulation of periodic NMR problems: Fast calculation of carousel averages, *Molec. Phys*. **95,** 879–890 (1998).
30. S. Dusold, Ph.D. thesis, University of Bayreuth (2000).
31. P. Hodgkinson and L. Emsley, Numerical simulations of solid-state NMR experiments, *Progr. Nucl. Magn. Reson. Spectrosc*. **36,** 201–239 (2000).
32. R. R. Ernst, G. Bodenhausen, and A. Wokaun, "Principles of Nuclear Magnetic Resonance in One and Two Dimensions," Clarendon, Oxford (1987).
33. http://www.epm.ornl.gov/pvm/.
34. F. James and M. Roos, MINUIT computer code, Program D-506, CERN, Geneva (1977).
35. M. Bechmann and A. Sebald, to be published.
36. X. Feng, Y. K. Lee, D. Sandström, M. Edén, H. Maisel, A. Sebald, and M. H. Levitt, Direct determination of a molecular torsional angle by solid-state NMR, *Chem. Phys. Lett*. **257,** 314–320 (1996).
37. M. Hohwy, H. J. Jakobsen, M. Edén, M. H. Levitt, and N. C. Nielsen, Broadband dipolar recoupling in the nuclear magnetic resonance of rotating solids: A compensated C7 pulse sequence, *J. Chem. Phys*. **108,** 2686–2694 (1998).
38. M. Carravetta, M. Edén, X. Zhao, A. Brinkmann, and M. H. Levitt, Symmetry principles for the design of radiofrequency pulse sequences in the nuclear magnetic resonance of rotating solids, *Chem. Phys. Lett.* **321,** 205–215 (2000).
39. M. Carravetta, M. Edén, O. G. Johannessen, H. Luthman, P. E. Verdegem, J. Lugtenburg, A. Sebald, and M. H. Levitt, submitted for publication.
40. M. Bechmann, X. Helluy, C. Marichal, and A. Sebald, submitted for publication.
41. M. Bechmann, X. Helluy, and A. Sebald, Selectivity of double-quantum-filtered rotational-resonance experiments on larger-than-two-spin systems, *in* "Perspectives on Solid-State NMR in Biology" (S. Kiihne and H. J. M. de Groot, Eds.), Kluwer, Dordrecht, The Netherlands (2001), in press.